Early symptom-associated inflammatory responses shift to type 2 responses in controlled human schistosome infection

Houlder, E.L.; Stam, K.A.; Koopman, J.P.R.; Koenig, M.H.; Langenberg, M.C.C.; Hoogerwerf, M.A.; ... ; Roestenberg, M.

INFECTIOUS DISEASE

Early symptom-associated inflammatory responses shift to type 2 responses in controlled human schistosome infection

Emma L. Houlder†, Koen A. Stam†, Jan Pieter R. Koopman, Marion H. König, Marijke C. C. Langenberg, Marie-Astrid Hoogerwerf, Paula Niewold, Friederike Sonnet, Jacqueline J. Janse, Miriam Casacuberta Partal, Jeroen C. Sijtsma, Laura H. M. de Bes-Roeleveld, Yvonne C. M. Kruize, Maria Yazdanbakhsh*†, Meta Roestenberg†

Schistosomiasis is an infection caused by contact with *Schistosoma*-contaminated water and affects more than 230 million people worldwide with varying morbidity. The roles of T helper 2 (T_H2) cells and regulatory immune responses in chronic infection are well documented, but less is known about human immune responses during acute infection. Here, we comprehensively map immune responses during controlled human *Schistosoma mansoni* infection using male or female cercariae. Immune responses to male or female parasite single-sex infection were comparable. An early T_H1-biased inflammatory response was observed at week 4 after infection, which was particularly apparent in individuals experiencing symptoms of acute schistosomiasis. By week 8 after infection, inflammatory responses were followed by an expansion of T_H2 and regulatory cell subsets. This study demonstrates the shift from T_H1 to both T_H2 and regulatory responses, typical of chronic schistosomiasis, in the absence of egg production and provides immunological insight into the clinical manifestations of acute schistosomiasis.

INTRODUCTION

Globally, more than 230 million people are infected with schistosomes, mainly *Schistosoma mansoni* and *Schistosoma haematobium* (*1*). Schistosomes undergo multiple developmental stages in the human host, causing stage-specific morbidity. Cercarial dermatitis occurs upon skin invasion, followed by acute schistosomiasis syndrome (Katayama fever) 2 to 7 weeks later, in response to migrating and maturing schistosomes (*2*–*5*). Severe disease manifestations occur in up to 10% of infected individuals during patent (egg-producing) infection, with eggs released into the vasculature becoming lodged in multiple organs, inducing a granulomatous response and varied clinical presentations (*6*). Sterilizing immunity does not develop against schistosomes, such that individuals can be rapidly reinfected upon exposure to contaminated water even after successful treatment with the schistosomocidal drug praziquantel (*7*). There is no approved vaccine for schistosomiasis, and vaccine design is hindered by a lack of understanding of natural immune responses to schistosomes, particularly during acute stages of infection, despite data in preclinical models identifying larval antigens as key vaccine targets (*8*). A better understanding of human immune responses during acute infection is critical to define correlates of protection and inform vaccine development.

Our understanding of immune responses in acute human schistosomiasis has been guided by a limited number of clinical and immunological studies. Clinical manifestations of acute schistosomiasis include fever, fatigue, cough, and eosinophilia (*2*). One endemic study looking at individuals with acute schistosomiasis (4 to 8 weeks after exposure) has shown enhanced production of T_H1 (T helper 1) cytokines [interleukin-1 (IL-1), tumor necrosis factor–α (TNFα), and interferon-γ (IFN-γ)] compared with patients with chronic schistosomiasis, who have enhanced production of the T_H2-associated cytokine IL-5 (*9*). In murine models, egg production is the major driver of type 2 immune responses in schistosomiasis (*10*), with a mixed type 1/type 2 response present in prepatent or single-sex *S. mansoni* infection (*11*–*13*). Schistosome worms exhibit marked morphological and transcriptional differences dependent on sex; however, whether this translates to altered immune phenotypes is unclear (*14*–*18*).

Precise mapping of human immune responses over time has only become possible after the establishment of a controlled *S. mansoni* infection model (*3*, *5*). In these studies, volunteers are infected with 10 to 30 single-sex cercariae before treatment at weeks 8 and 12 (female cercariae) or week 12 (male cercariae) with praziquantel (*3*, *5*). Acute schistosomiasis symptoms, including fever, headache, and myalgia, were observed in 14 of 30 participants between weeks 3 and 7 after infection, with 9 of these symptomatic participants experiencing a severe adverse event (*3*, *5*). Similar immune responses were found in both studies, with an increased serum concentration of the inflammatory chemokine CXCL10 at week 4 and increased schistosome-specific T_H1 (IFN-γ) and T_H2 (IL-4/IL-5/IL-13) cytokines (*3*, *5*). Although informative, these studies lacked both depth and breadth of the immune outputs measured, focusing on a few circulating cytokines, and antigen-specific cytokine production by $CD4^+$ T cells. Further immune profiling is therefore required to understand cellular and cytokine changes during the initial phases of schistosome infection.

Here, we used mass cytometry to broadly and specifically profile cellular immune responses, including B cells, T cells, innate lymphoid cells (ILCs), and myeloid cells, in the first months of *S. mansoni* infection. Alterations in frequency and phenotype of peripheral blood mononuclear cells (PBMCs) were measured at weeks 4, 8, and 12 after infection with cellular responses supported by multiplex serum cytokine analysis. Comparisons with baseline participant samples and between symptomatic and asymptomatic participants were performed to deepen our understanding of the pathogenesis of acute schistosomiasis syndrome.

Leiden University Center for Infectious Diseases, Leiden University Medical Center, Albinusdreef 2, 2333ZA Leiden, Netherlands.
*Corresponding author. Email: m.yazdanbakhsh@lumc.nl
†These authors contributed equally to this work.

RESULTS

Symptom severity, and not cercarial sex or dose, explains most variation in cellular phenotype during infection

To understand immune changes during schistosome infection, PBMC and serum samples were analyzed from two independent studies, infection with male *S. mansoni* cercariae ($n = 14$, samples analyzed at weeks 0, 4, and 8 after infection) or infection with female *S. mansoni* cercariae ($n = 13$, samples analyzed at weeks 0, 4, 8, and 12 after infection) (Fig. 1A) (*3*, *5*). The choice of time points was informed by clinical findings, with acute schistosomiasis symptoms occurring between weeks 3 and 7 after infection (Fig. 1A) (*3*, *5*). Because these were parts of dose-escalating clinical safety trials, volunteers were experimentally exposed to 10 male or female cercariae ($n = 6$), 20 male or female cercariae ($n = 18$), or 30 male cercariae ($n = 3$) (*3*, *5*). PBMCs were stained with a comprehensive panel encompassing 35 phenotyping markers, acquired, preprocessed, and then clustered via self-organizing map (SOM), followed by hierarchical clustering (Fig. 1B). We were able to categorize 70 immune cell clusters (Fig. 1C) on the basis of marker expression. These clusters were segregated into seven lineages: $CD4^+$ T cells, $CD8^+$ T cells, γδ T cells, unconventional T cells, B cells, ILCs, and myeloid cells (Fig. 1D).

We performed principal components analysis (PCA) on the cluster frequencies, whereby we included all individuals on all time points. The first two principal components were able to explain 33% of the variation in the data (Fig. 1E). Notably, a group of 12 data points, all from week 4 (depicted as green points), were separated from the rest on both axes (Fig. 1E). Coloring the data points by key clinical factors, including cercarial sex, dose, time, and symptoms, allowed us to investigate their relative contributions to the principal components. Neither cercarial sex (Fig. 1F) nor dose (fig. S1) seemed to explain the largest block of variance. We formally tested for cercarial sex, with only two cell clusters changing differently over time between male and female infections (fig. S2). These were cluster 25 (c25), basophils, which were increased at week 8 in male but not female infection, and c49, $CD14^-CD16^-$HLA-DR^+ conventional dendritic cells, which increased at week 4 in female but not male infection (fig. S2).

Next, we checked whether symptoms were associated with specific samples that were grouped separately in the PCA at week 4. Individuals who experienced only mild/moderate symptoms of acute schistosomiasis clustered with the asymptomatic group, whereas most individuals who experienced at least one severe symptom clustered separately (Fig. 1G). For further analysis, we grouped individuals with only mild or moderate symptoms with the asymptomatic participants, as explained in Fig. 1H. These groups will be referred to as volunteers with either severe symptoms or no/mild symptoms. This categorization provides increased confidence in a correct diagnosis of acute schistosomiasis syndrome, which consists of a variety of nonspecific symptoms, including headache, fever, and malaise (*3*, *5*).

Inflammatory cellular responses, enhanced in individuals with severe symptoms, are observed at week 4

We next asked how immune responses changed during infection, taking into account whether individuals had experienced acute schistosomiasis symptoms. At the lineage level, no differences were seen over time in individuals with no/mild symptoms. However, in individuals with severe symptoms at week 4, an altered immune composition is readily apparent. Myeloid cells tend to increase, whereas CD8 T and B cell lineages decrease, with other time points remaining relatively stable compared with baseline (Fig. 2A).

To formally test changes in the immune cell composition, we used a generalized linear mixed model to inquire how immune cell clusters changed over time and whether these changes differed between symptom severity groups. Notably, changes were only observed at the cluster level, with a later investigation revealing no significant changes when clusters were combined into classical immune cell subsets (fig. S3). Two CD4 T cell clusters, c10 and c11, increased significantly [false discovery rate (FDR) = 0.03 and 0.01] in all volunteers (Fig. 2B, left); however, a significantly stronger increase (FDR = 0.002 and 0.002) in the abundance of these clusters was found for volunteers with severe symptoms (Fig. 2B, right) in comparison with volunteers with no/mild symptoms. Clusters c10 and c11 have similar phenotypic immune markers and appear to be activated HLA-DR^+ effector memory (EM; $CD45RA^-CCR7^-CD45RO^+$) CD4 T cells that differ in expression of CD38 (Figs. 1C and 2C). Alongside EM cluster expansion, we detected the beginnings of a regulatory response, with increased HLA-DR^+ CD4 regulatory T cells (T_{regs}) (c6) (Fig. 2D), although the magnitude of this expansion was less compared with the EM T cells.

Innate inflammatory responses were also apparent in the severe symptomatic participants in contrast with the volunteers with no/mild symptoms. Expansion of an activated $CD38^+$ HLA-DR^{high} classical monocyte ($CD14^+CD16^-$) cluster (c34) was observed in severe symptomatic individuals (Fig. 2E). Accompanying this was a decrease in a $CD38^-$ HLA-DR^{mid} classical monocyte ($CD14^+CD16^-$) cluster (c30), suggestive of a transition toward greater activation in the classical monocyte compartment in those developing severe symptoms (Fig. 2E and figs. S4A and S5). PCA loadings (fig. S1) reveal these myeloid and CD4 T cell clusters (c10, c11, c34, and c6) to be responsible for the observed separation of severe symptomatic week 4 samples in Fig. 1G. Last, cytotoxic $CD56^{dim}$ $CD16^+$ natural killer (NK) cells (*19*), which tended to decrease in volunteers with no/mild symptoms, were significantly increased (FDR = 0.001) at week 4 in severe symptomatic individuals (Fig. 2F).

In addition to increases in the aforementioned clusters, a number of lymphocyte clusters decreased at week 4 in symptomatic individuals. Potentially, in response to chemokine signals, there was a reduction in $CXCR5^+CD38^-$ memory B cells (c13) at week 4 in individuals with severe symptoms (Fig. 2G). In addition, a modest reduction in two $CD127^+$ EM CD4 T cell clusters at week 4 was observed in severely symptomatic individuals (Fig. 2H and fig. S4E). An NK and γδ T cell cluster also decreased (fig. S4, C and D). Most notable was a decrease in multiple CD8 T cell clusters (c50, c35, c65, c58, c41, and c26) (Fig. 2I, individually in fig S4B). To understand this reduction, we checked whether these clusters expressed similar phenotypic markers. The reduced CD8 T cell clusters had heterogeneous expression of memory and naïve markers (CD45RO, CCR7, and CD45RA); however, all were killer cell lectin-like receptor G1 $(KLRG1)^+$, with the majority expressing CXCR3, which binds interferon-inducible ligands including CXCL9 and CXCL10 (*20*). It is possible, therefore, that the reduction in CD8 T cell clusters was in response to increases in circulating CXCR3 ligands during the inflammatory response, observed in serum. Together, cellular changes at week 4 are characterized by alterations in clusters from multiple cell lineages in symptomatic individuals, with expansion of mainly CD4 T cell

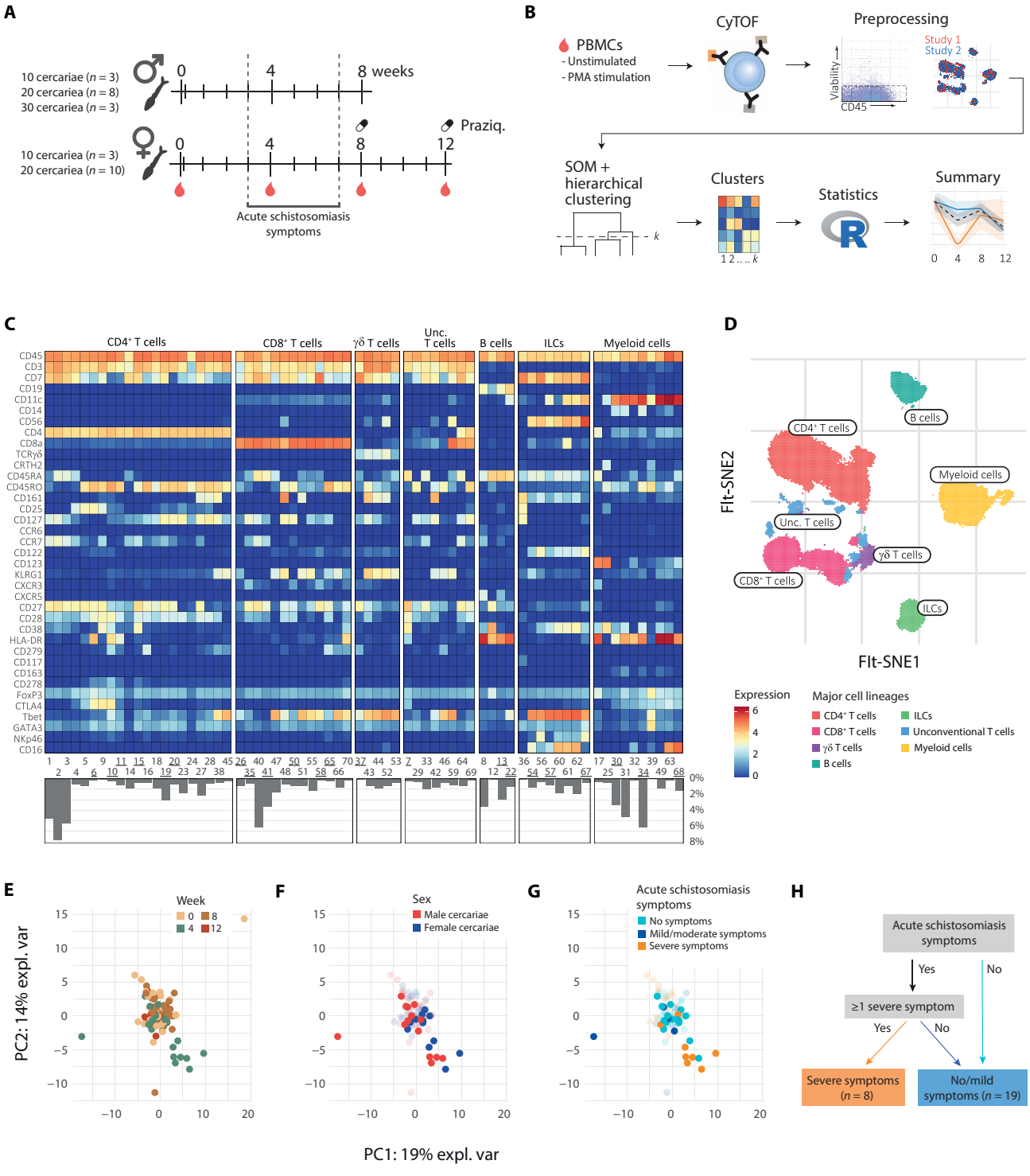

Fig. 1. Overview of study design and cellular changes during controlled *S. mansoni* infection. (**A**) Graphical representation of the trial design and (**B**) analysis pipeline. (**C**) Top: Heatmap of identified cell clusters after CyTOF analysis of unstimulated samples based on SOMs and hierarchical clustering. Each tile depicts the median expression of a given marker (*y* axis) for a specific cluster (*x* axis) across all time points. Bottom: Percentage of the total cells of a given cluster divided by total CD45$^+$ cells. Clusters that were found significantly different from the linear mixed model are underscored for readability. (**D**) Binned representation of the t-SNE map with CD45$^+$ cells, colored by lineage of most cells in the bin. (**E** to **G**) A multilevel PCA was applied to individual samples, one sample being one participant at a specific time point, based on cluster frequencies (scaled to unit variance). The PCA was colored on the basis of (E) time point, (F) sex, or (G) symptoms, with time points 0, 8, and 12 shown at 15% transparency in (F) and (G) to highlight week 4 (opaque). (**H**) Flow chart for classification of individuals into two groups; volunteers with severe symptoms or no/mild symptoms. All analyses were performed on $n = 27$ individual participants.

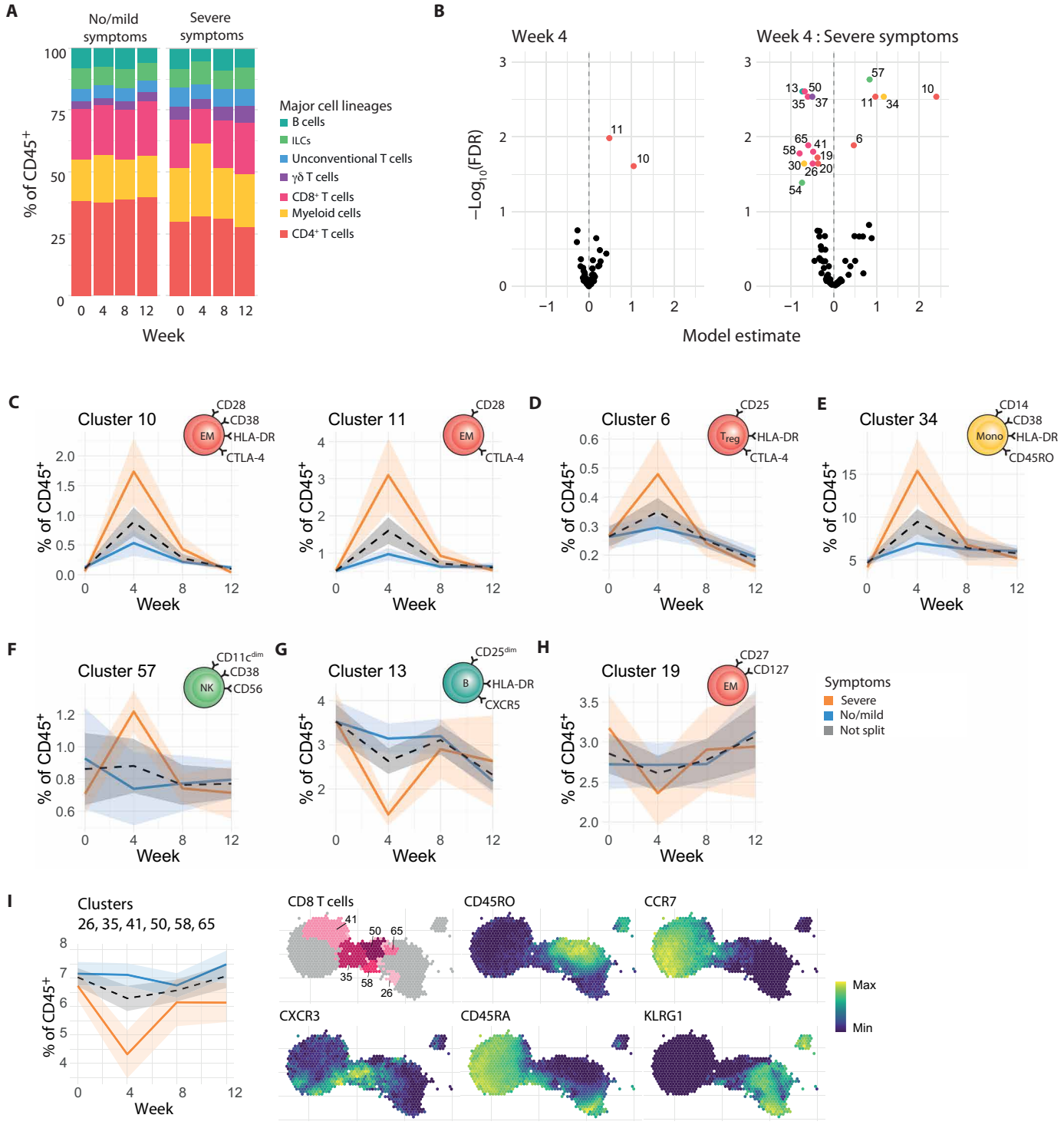

Fig. 2. Characterization of cellular kinetics at week 4 of *S. mansoni* infection. (**A**) Stacked bar chart of lineage frequencies in individuals with no/mild symptoms or severe symptoms. Each bar section represents the mean frequency of that cell lineage for the corresponding group. (**B**) Volcano plots showing the model estimates and corresponding adjusted *P* values [$-\log_{10}$(FDR)] of the week 4 time point term (left) and the interaction term between week 4 and symptoms (right). Estimates are derived from a binomial linear mixed model, where each cluster is modeled separately. All analyses were performed on $n = 27$ individual participants. Each point represents a cluster, and clusters with FDR values of <0.05 are colored by lineage and labeled with cluster ID. (**C** to **I**) Ribbon plots depicting mean (lines) frequency and SEM (shaded area) of specified clusters. Cluster frequencies are given as a percentage of $CD45^+$ cells and split/colored by symptom status. (I) Right: Binned representation of the CD8 cell island on the t-SNE map. Hexagonal bins colored by cluster or expression of selected markers. Clusters significantly altered at week 4 are colored pink, and nonaltered clusters are in gray. Left: Ribbon plots showing frequency of selected CD8 clusters (c50, c30, c65, c58, c41, and c26) over time.

clusters, monocyte activation, and decreases in chemokine receptor–expressing CD8 T and B cells.

Mature and regulatory cellular immune responses are observed at weeks 8 to 12

At week 8 after infection, there were fewer significantly altered cell clusters (Fig. 3A), with only one cluster elevated after treatment (week 12). Moreover, no significant interactions were observed between time and symptoms. This is in line with the subsiding of acute schistosomiasis symptoms by week 7 (*3*, *5*) and indicates that the exaggerated inflammatory response observed in severe symptomatic individuals does not lead to altered long-term responses in the presence of adult worms.

Cellular responses at week 8 tended to have a more mature or regulatory phenotype. There was an increase in the c7 cluster of $CD38^+$ double-negative (DN) ($CD4^-CD8^-$) T cells (Fig. 3B), which have previously been shown to inhibit T_H1 responses (*21*–*23*). In addition, an increase in atypical $CD11c^+Tbet^+CD38^-$ memory B cells (Fig. 3C) was observed, which are known to expand in chronic infections, aging, or autoimmunity (*24*, *25*). Last, at week 8 after infection, there

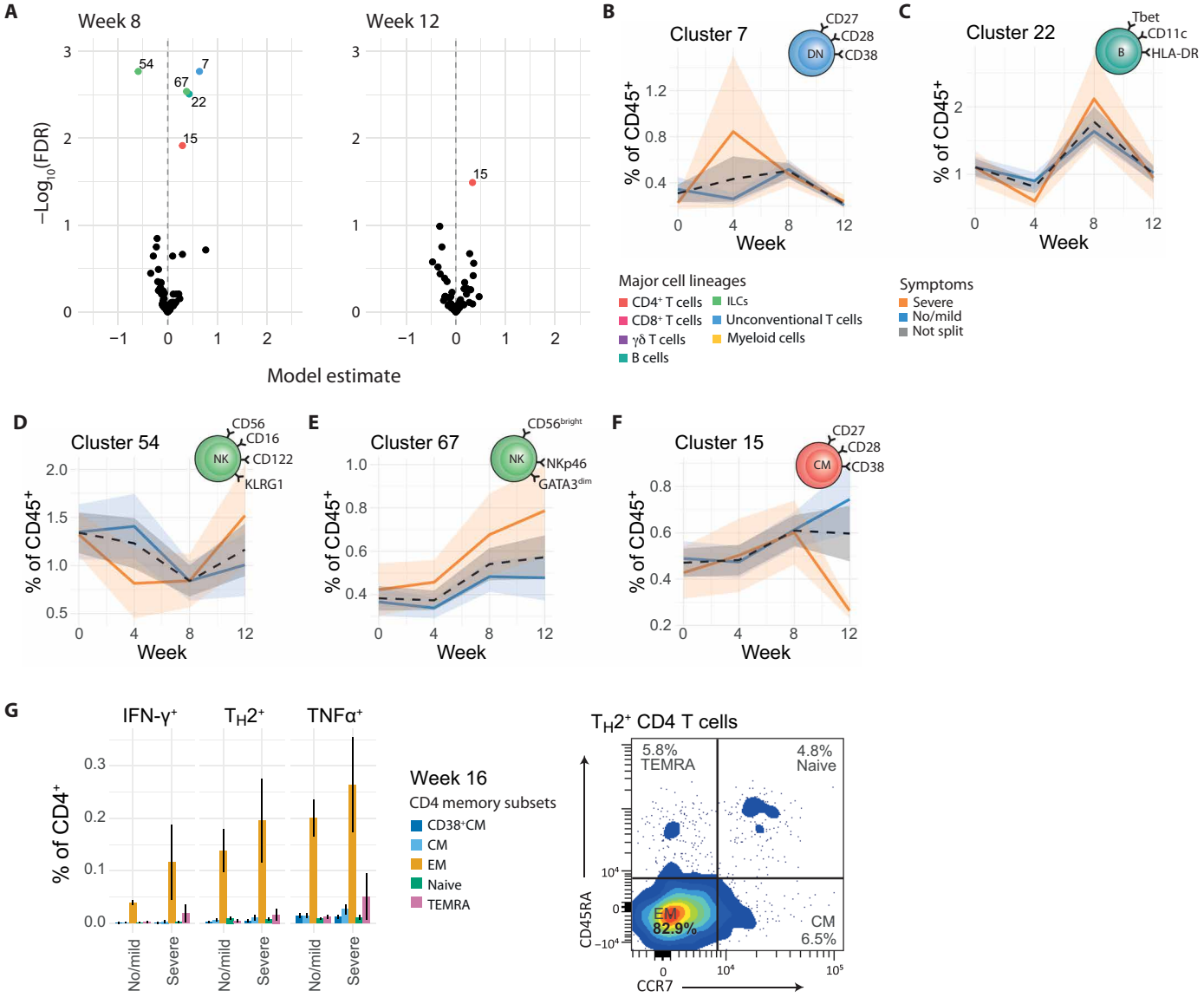

Fig. 3. Characterization of cellular kinetics at weeks 8 to 12 of *S. mansoni* infection. (**A**) Volcano plots showing the estimates and minus log-scaled FDR-corrected *P* values [$-\log_{10}$(FDR)] of the week 8 time point (left) and week 12 time point (right). Values derived from a binomial linear mixed model. Each point represents a cluster, and clusters with FDR values of <0.05 are colored by lineage and labeled with cluster ID. (**B** to **F**) All colored ribbon plots show cluster frequencies as a percentage of $CD45^+$ cells. These are split and colored by symptoms, with lines representing the mean value and ribbon shading ± SEM. Ribbon plots showing frequency of (B) c7, (C) c22, (D) c54, (E) c67, and (F) c15 over time. All analyses were performed on $n = 27$ individual participants. (**G**) PBMCs from week 16 after infection ($n = 12$) were stimulated with AWA or medium before analysis of intracellular cytokines via flow cytometry. Grouped bar plot represents AWA-specific cytokines within memory subtypes: EM, effector memory cells reexpressing CD45RA (TEMRA), and CM. Representative flow cytometry plot shows the distribution of T_H2 cytokines within CD4 T cell memory populations, showing all AWA-stimulated samples concatenated. Frequencies on plot represent the percentage of the total T_H2^+ CD4 T cell population.

was a significant decrease in a cluster of cytotoxic $CD56^+$ $CD16^+$ NK cells (FDR = 0.002) (Fig. 3D) and an increase in regulatory $CD56^{bright}CD16^-$ NK cells (FDR = 0.003) (Fig. 3E) (*26*, *27*). The existence and dynamics of key clusters (c10/11, c34, c7, and c22) that changed at both weeks 4 and 8 were independently confirmed by flow cytometry (figs. S5 and S6).

Posttreatment changes at week 12 were tested only in the female cercaria infection model. We observed that cellular responses tended to return to baseline after praziquantel treatment. The one exception to this was a rare $CD38^+$ central memory (CM; $CD45RA^-CCR7^+CD45RO^+$) CD4 T cell cluster (c15), which increased at week 8 and remained elevated until week 12 (Fig. 3, A and F). To understand whether these $CD38^+$ CM cells (c15) represented a key memory population, we performed further analysis at week 16 (after treatment) (Fig. 3E and fig. S7). We were able to confirm the trend for reduced $CD38^+$ CM cells at week 16 in severe symptomatic individuals (fig. S7A). Notably, however, although $CD38^+$ CM cells were able to produce T_H1 (IFN-γ and TNFα) and T_H2 cytokines in response to adult worm antigen (AWA), most AWA-specific cytokines were produced by EM T cells (Fig. 3G).

Cellular cytokines shift from an initial T_H1 dominance at week 4 to a T_H2 and regulatory response at week 8

Having established cellular dynamics during infection, we next investigated functional properties of these cells by measuring cytokine production after stimulation with phorbol 12-myristate 13-acetate (PMA)/ionomycin. This approach was chosen to allow us to assess how schistosome infection alters the cytokine production potential of multiple immune cell lineages, irrespective of antigen specificity. We considered the global cytokine production as the total amount of cytokine-positive cells divided by all $CD45^+$ cells. At week 4 after infection, the only significantly increased cytokines were T_H2 (IL-13/IL-4/IL-5) (FDR = 0.02), which remained elevated up to week 8 (FDR = 0.03). At week 8, a mixed response was observed, with a decrease in the proinflammatory cytokine TNFα (FDR = 0.02) and an increase in IL-6 (FDR = 0.02) and the regulatory cytokine IL-10 (FDR = 0.002) (Fig. 4A). No significant alteration in IFN-γ, IL-2, or IL-17 expression was observed (Fig. 4A). To gain a more in-depth understanding of cytokine responses, clustering was performed on stimulated cells, resulting in 70 clusters, 43 of which produced cytokines. The phenotypes of these clusters are summarized in Fig. 4B. To investigate and formally examine changes in frequency of cytokine-expressing cells, we used a similar binomial linear mixed model to inquire how immune cell clusters changed at weeks 4 and 8 after infection and whether these changes differed in symptomatic individuals.

At week 4 after infection, an increase in $HLA\text{-}DR^+$ EM T cells, as well as a decrease in a number of CD8 T cell clusters, was observed in individuals with severe symptoms, which corresponds to our findings in the unstimulated panel. At week 4, there was an increase in c33, an $HLA\text{-}DR^+$ EM T cell, which was elevated in severe symptomatic participants (Fig. 4D), phenotypically similar to the $HLA\text{-}DR^+$ EM T cell we observed elevated in the unstimulated panel. These $HLA\text{-}DR^+$ EM T cells were all $IFN\text{-}\gamma^+$, with a minority $IL\text{-}2^+$ and T_H2^+ as well (Fig. 4D). Reduced CD8 T cell clusters (Fig. 4E and fig. S8, A and B) expressed T_H1 cytokines IFN-γ and TNFα. Together, T_H1/T_H2 cytokine–expressing CD4 T cells increased, whereas type 1 cytokine–expressing CD8 T cells decreased at week 4, with a higher magnitude of both effects in symptomatic individuals.

In contrast with our unstimulated cellular findings, most changes in cytokine-producing clusters were observed at week 8 after infection (Fig. 4C). Notably, as we saw in the unstimulated panel, cluster frequencies in severe symptomatic and no/mild symptomatic individuals converged at week 8 after infection, with no long-term effects of the earlier enhanced inflammatory response in severe symptomatic individuals. Specifically, we observed that $CD38^+$ DN T cells, which we observed expanding in the unstimulated panel Fig. 3B, express the regulatory cytokine IL-10 (Fig. 4F, confirmed fig. S6D), supporting our proposition that these cells play a regulatory role. A steady increase in the T_H2 response was observed in the CD4 T cell compartment, with an increase in a number of $CD4^+$ T cell clusters that expressed T_H2 cytokines, and coexpressed IL-2, IFN-γ, and TNFα (Fig. 4, G and H, and fig. S8, C and D). Decreases in a type 1 cytokine (IFN-γ and TNFα)–expressing CD8 T cell cluster and two NK cell clusters were observed (Fig. 4, I to K). Together, the symptom-related T_H1/T_H2 CD4 T cell response at week 4 was replaced at week 8 by a symptom-independent increase in T_H2-expressing CD4 T cell clusters and IL-10–expressing DN T cells, with a decrease in type 1 cytokine–expressing CD8 T cells and NK cell clusters.

Inflammatory circulating cytokines peak at week 4 in individuals with severe symptoms, with increased dominance of regulatory IL-10 at weeks 8 to 12

To complement our cellular findings, we performed a 96-plex immunoassay on serum cytokines and chemokines. In line with our cellular results, we observed the most changes in serum cytokines at week 4 after infection, with most proteins being only elevated in individuals with severe symptoms and not for asymptomatic volunteers, with the exception of IFN-γ (Fig. 5A). In the individuals with severe symptoms, we saw elevation of IFN-γ, interferon-induced chemokines (CXCL11, CXCL9, and CXCL11), other type 1 inflammatory mediators (TNF), and factors involved in cell survival, migration, and differentiation [osteoprotegerin (OPG), leukemia inhibitory factor (LIF), and CUB domain-containing protein 1 (CDCP1)] (Fig. 5A). Most cytokines upregulated at week 4 remained significantly elevated at week 8 (Fig. 5B). In these individuals, serum cytokines tended to decrease between weeks 4 and 8, whereas cytokines in individuals with no/mild symptoms tended to increase or remain constant, leading to equivalent cytokine concentration by week 8 (Fig. 5C). In contrast to our cellular results, where increases in T_H2 cytokines were observed at week 8, we did not observe any significant changes in type 2 cytokines measured (IL-4, IL-13, and IL-5). At week 8 after infection, there was an elevation of the regulatory cytokine IL-10, which was also the only cytokine that remained significantly elevated at week 12 after infection compared with baseline (FDR = 0.02) (Fig. 5B). To further understand this potential shift to a regulatory phenotype, we undertook further analysis of T_{reg} clusters and checkpoint markers [cytotoxic T-lymphocyte associated protein 4 (CTLA-4) and programmed cell death protein 1 (PD-1)] on CD4 T cells; however, these were not significantly increased at weeks 8 to 12 (fig. S9).

Correlation analysis was then performed to understand the interaction between serum and cellular cytokine responses at each time point (Fig. 5D). Stimulated cell clusters and serum cytokines were chosen for this analysis if they had been shown to significantly change over time or have an interaction with acute schistosomiasis symptoms (Fig. 4C). Significant correlations were observed at weeks 4 and 8 during schistosome infection and not at baseline (fig. S10). At week 4, $IFN\text{-}\gamma^+$ $HLA\text{-}DR^+$ EM T cells (c33) were positively correlated with

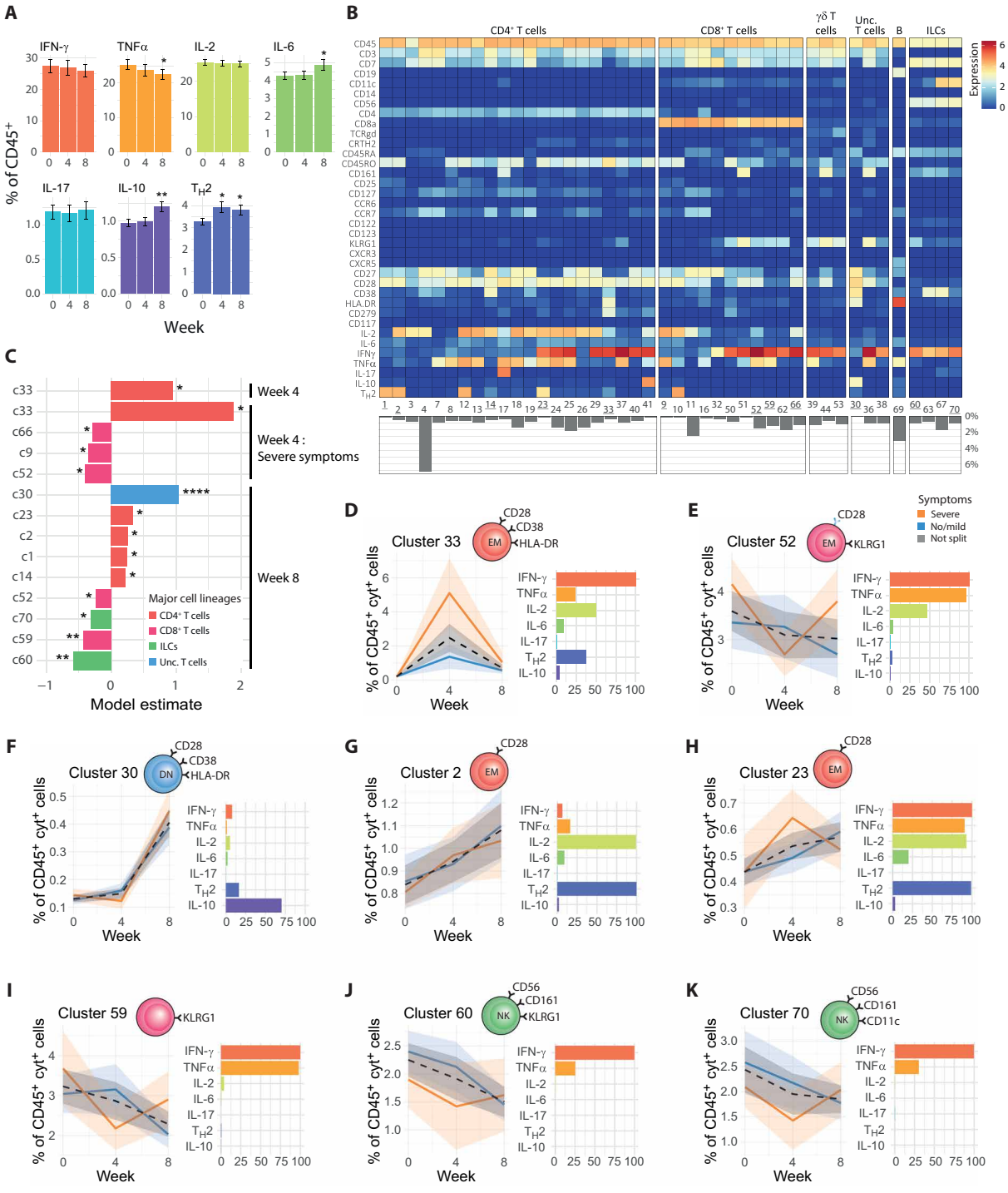

Fig. 4. Characterization of cellular cytokine expression during *S. mansoni* infection. Cytokines were measured in PMA/ionomycin-stimulated PBMC samples ($n = 27$ individual participants). (**A**) Cytokine frequencies in total CD45$^+$ cells. A binomial linear mixed model was used to determine changes from baseline. Error bars show the SEM. Uncorrected P values summarized in graphs as follows: *$P < 0.05$ and **$P < 0.01$. (**B**) Heatmap of identified cell clusters after CyTOF analysis of stimulated samples based on SOM and hierarchical clustering. Only cytokine-expressing cell clusters are shown, with clusters in which less than 50% of the cells express any cytokine excluded. Each tile depicts the median expression of a given marker (y axis) for a specific cluster (x axis) across all time points. Bottom: Percentage of the total cells of a given cluster divided by total CD45$^+$ cells. (**C**) Bar chart showing values derived from a binomial linear mixed model comparing cluster frequency over time and in relation to symptoms. Clusters with significant changes (FDR-corrected $P < 0.05$) over time, with or without symptom interaction, are shown. Bars are colored by lineage and labeled with cluster ID. (**D** to **K**) All colored ribbon plots show cluster frequencies (c33, c52, c30, c2, c23, c59, c60, and c70) as a percentage of total CD45$^+$ cytokine$^+$ cells. These are split and colored by symptoms, with lines representing the mean value and ribbon shading ± SEM. Cytokine expression in each cluster is shown in the bar chart, colored by cytokine. All analyses were performed on $n = 27$ individual participants. FDR-corrected P values summarized in graphs as follows: *$P < 0.05$, **$P < 0.01$, and ****$P < 0.0001$

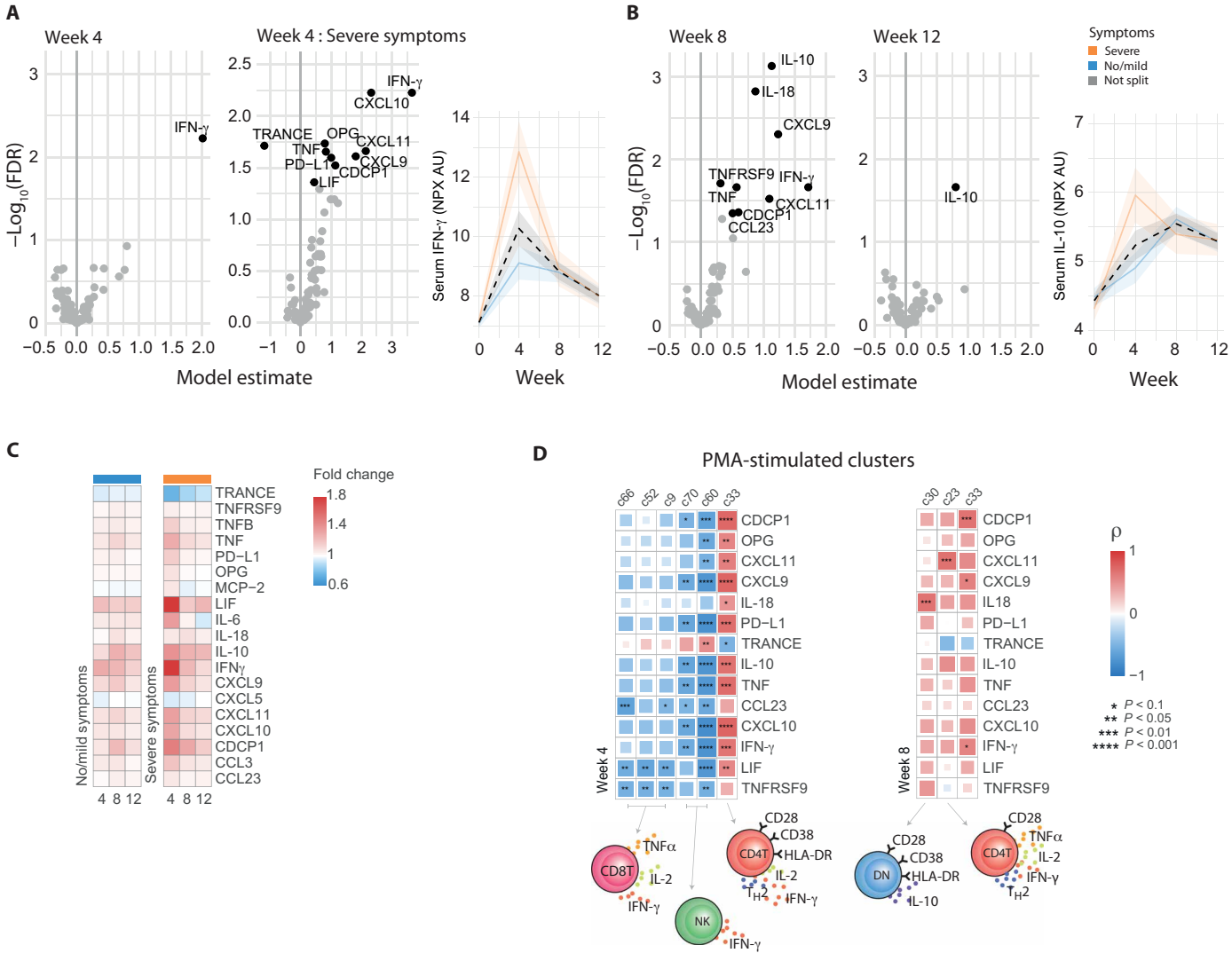

Fig. 5. Characterization of serum cytokine kinetics during *S. mansoni* infection. (**A**) Volcano plots showing the estimates and minus log-scaled FDR-corrected *P* values [$-\log_{10}$(FDR)] of the week 4 time point term (left) and the interaction term between week 4 and symptoms (middle). Ribbon plot showing serum IFN-γ over time (right). (**B**) Volcano plots showing the estimates and minus log-scaled FDR-corrected *P* values [$-\log_{10}$(FDR)] of the week 8 time point term (left) and the week 12 time point term (middle). Ribbon plot showing serum IL-10 over time (right). All values in volcano plots derived from a linear mixed model of normalized protein expression (NPX) values (AU on $\log_2$ scale). Each point represents a cluster, and clusters with FDR values of <0.05 are colored by lineage and labeled with cluster ID. Ribbon plots are split and colored by symptoms, with lines representing the mean value and ribbon shading ± SEM. (**C**) Summary heatmaps showing mean fold change from week 0 of serum cytokines, split by symptomatic and asymptomatic individuals. Rows represent time point (weeks), and columns represent serum cytokines. (**D**) Correlation matrices comparing frequencies of cell clusters (rows) and serum cytokines (columns) at weeks 4 and 8. Color and size of squares are proportional to the Spearman's ρ correlation coefficient, with red indicating a negative correlation and blue indicating a positive correlation. Serum cytokine analyses were performed on $n = 30$ individual participants, with correlations performed on $n = 27$ participants to match cellular data. Cell clusters and serum cytokines were selected to have significantly altered with time or symptoms, at a FDR of <0.1. Significant correlations are shown: *$P < 0.1$, **$P < 0.05$, ***$P < 0.01$, and ****$P < 0.001$

most inflammatory serum cytokines, including IFN-γ. At the same time, a negative correlation in NK cell clusters c60 and c70 and the same inflammatory cytokines was seen (Figs. 4, J and K, and 5D). Together, this suggests a concerted response regulating the observed decrease in NK cells and increase in IFN-γ^+ HLA-DR$^+$ EM T cells at week 4 in symptomatic individuals. By contrast, the decrease in CD8 clusters (c9, c52, and c66) seen at this time point was negatively correlated to the cytokines CCL23, LIF, and TNF receptor superfamily member 9 (TNFRSF9), which have been proposed to have an inhibitory effect on CD8 T cells (Fig. 5D) (*28*–*30*). Fewer significant correlations were observed at week 8. Notably, serum IL-18 was significantly positively correlated to CD38$^+$ DN T cells (FDR = 0.01), and serum CXCL11 was significantly positively correlated to T_H2/IFN-γ^+/TNFα$^+$ EM T cell c23 (FDR = 0.01) (Fig. 5D), potentially suggestive of functional relationships between these cytokines and expansion of these cell clusters at week 8 after infection. Integrating cellular and serum cytokine responses has therefore provided insight into different networks that regulate the early inflammatory response at week 4 and the increasingly mature response at week 8.

DISCUSSION

This study has comprehensively delineated cellular and cytokine responses in the first 2 months of schistosome infection, combining results from two single-sex (male or female) controlled human infection studies. Use of mass cytometry has allowed us to identify cell clusters across seven lymphoid and myeloid lineages in stimulated and unstimulated settings, complemented by a multiplex immunoassay to assess serum cytokine responses. Inflammatory responses, including serum IFN-γ and related proinflammatory cytokines, T_H1/T_H2 cytokine–producing HLA-DR$^+$ EM T cells, and activated monocytes, were elevated at week 4 in symptomatic individuals. By week 8 after infection, responses in individuals with severe symptoms and no/mild symptoms had converged, with an expansion of regulatory IL-10$^+$ DN T cells, atypical CD11c$^+$ memory B cells, and an increase in T_H2 cytokine–producing CD4 T cells observed in all symptom groups. Posttreatment immune responses returned to baseline, with the exception of serum IL-10 and a CD4 CM T cell cluster that remained elevated. Throughout infection, we have shown only minor differences in immune response between female and male single-sex infections. This finding is in line with the initial immunological analysis we have performed on the separate controlled human infection studies (*3*, *5*) and a recent murine study that found no immunological differences in chronic male or female single-sex infection (*14*). However, it is still unexpected in the context of prior papers that have shown sex-related differences in immune priming, as well as the known morphological and transcriptional differences between male and female worms (*15*–*18*).

At week 4, during the peak of reported symptoms, there were marked and previously undescribed alterations in specific systemic immune cell clusters (*3*, *5*). Although the exact timing of *S. mansoni* development in humans is unknown, rapid intramammalian growth of the parasite (from 1 to 5 mm) occurs between weeks 3 and 4 of infection, potentially accompanied by exposure of pathogen-associated molecular patterns (*31*, *32*). In response, we have observed an expansion of activated CD38$^+$ classical monocytes, particularly in symptomatic individuals. This monocyte phenotype has been previously reported in symptomatic bacterial, viral, and autoimmune responses (*33*–*35*). In addition, we observed expansion of T_H1/T_H2 cytokine–expressing HLA-DR$^+$ EM CD4 T cells, which have been shown to expand in acute inflammation, including during active tuberculosis infection (*36*). HLA-DR expression in CD4 T cells may derive from trogocytosis of activated monocytes, with HLA-DR enhancing T cell receptor signaling, survival, and T_H2 cytokine expression (*37*, *38*). Our cellular findings were supported by serum inflammatory cytokines (including IFN-γ, CXCL10, and TNFα), which are elevated under other acute inflammatory conditions and can directly induce symptoms such as fever (*39*, *40*). This suggests that the proinflammatory responses at week 4 may represent a stereotypical acute response to infectious agents, potentially induced by increased foreign schistosome antigen exposure and responsible for acute schistosomiasis symptoms. By performing correlation analyses between circulating and cellular cytokines, we gained insight into the relationship between immune responses. Some of these relationships, including the positive correlation between IFN-γ$^+$ EM T cells (c33) and CXCL10, could be expected from prior literature (*39*, *41*). Others, such as the negative correlations between CD8 cell cluster at week 8 and the circulating cytokines CCL23, LIF, and TNFRSF9, are less well described and warrant further investigation in other inflammatory situations.

Later in infection (from week 8), responses in individuals who had experienced severe symptoms and those with no/mild symptoms converged, with an increased T_H2 response and muted serum type 1 cytokines. Conventional dogma states that egg production is required for T_H2 responses in schistosomiasis (*9*, *10*, *42*). This finding has recently been challenged by studies demonstrating T_H2 responses to immature worms in the first month of infection before egg deposition (*11*, *13*, *43*). Our work furthers these findings, showing continued enhancement of T_H2 responses up to week 8 after infection, in a single-sex egg-free system. Through in-depth analysis, we were able to pinpoint this expression to CD28$^+$ EM CD4$^+$ T cells. The convergence of immune responses in individuals with severe symptoms and no/mild symptoms at week 8 could be due to increased immune regulation in symptomatic individuals, thus down-regulating their response. Here, similar to our prior works (*3*, *5*), we found an increase in a Foxp3$^+$ T_{reg} cluster in symptomatic individuals. Independent of symptoms, all participants showed an enhanced regulatory response at week 8, with increased serum IL-10. IL-10 has crucial regulatory and host-protective roles in schistosomiasis (*44*–*47*). We identified CD38$^+$ DN T cells as key producers of IL-10 and revealed a correlation between this subset and the concentration of IL-18 (*48*). Several studies have linked DN T cells to a suppressive function in noninfectious diseases, including reducing the ability of CD4$^+$ T cells to produce T_H1 cytokines (*21*–*23*). There is also evidence for a regulatory shift in the B cell compartment at week 8, with an expansion of atypical memory CD11c$^+$ B cells. This B cell subset is expanded in chronic exposure, including during parasite (malaria) infection, with anergic characteristics and diminished B cell receptor signaling (*24*, *25*). Further research is needed to understand the regulatory components of this system for comparison with the endemic system. At the posttreatment time point (week 12), immune responses tended back to baseline, with few long-term changes. Only the regulatory cytokine IL-10 in serum and a CD38$^+$ CM T cell cluster (c15) remained elevated. Notably, worm-specific memory responses were still present after infection, with EM CD4 T cells as the main responders. The relatively muted response at week 12 contrasts with studies in endemic areas, which have observed elevated immune responses after praziquantel treatment (*49*, *50*).

The use of a high-dimensional and semiunsupervised approach has allowed us to reveal changes in immune cells and cytokines, such as DN T cells and serum IL-18, that have not previously been a focus of schistosome research and warrant further study. The applicability of our study to the endemic situation is limited by the single-sex nature of the model and the acute nature of the controlled human infection, where schistosome-induced immune hyporesponsiveness has not yet developed (*51*, *52*). Our study, and particularly the inflammatory response at week 4, has particular relevance for understanding the pathogenesis of acute schistosomiasis in travelers to endemic countries (*53*). The week 8 response aligns best with our understanding of responses in endemic infection, where acute symptoms are rare (*54*, *55*). A limitation of this study is insufficient power to comprehensively assess differences due to age and sex or gender of human participants, as well as potential underestimation of week 12 responses due to the lower sample size at this time point, with only female infection samples ($n = 13$) measured. Moreover, we do not know whether the immune changes highlighted here are protective against infection or symptoms in schistosomiasis. However, by highlighting the key players in the initial immune response in schistosomiasis, this work provides direction for future studies to better

understand protective immune responses and therefore guide schistosome vaccine development. By identifying the key immune cell clusters that play a role in schistosomiasis, it is now possible to specifically target these cells when designing vaccines or investigating correlates of protection.

MATERIALS AND METHODS

Study design

Samples in this study were part of two dose-escalating clinical safety trials of controlled human schistosome infection. In the first study (NCT02755324), 17 volunteers were infected with 10 ($n = 3$), 20 ($n = 11$), or 30 ($n = 3$) male *S. mansoni* cercariae, as previously described (*3*). Three volunteers were not included in the cellular analysis detailed here because of low cell numbers; therefore, we analyzed samples from 14 volunteers, exposed to 10 cercariae ($n = 3$), 20 cercariae ($n = 8$), or 30 cercariae ($n = 3$). In the second study (NCT04269915), 13 volunteers were infected with 10 ($n = 3$) or 20 ($n = 10$) female *S. mansoni* cercariae, as previously described (*5*). Samples from all volunteers in this female infection study were analyzed. These studies were powered (sample size determination) studies to achieve the primary outcomes (infection and symptoms), as detailed previously (*3*, *5*). Volunteers were treated with praziquantel (40 mg/kg) at week 12 in the male infection study and at weeks 8 and 12 (60 mg/kg) in the female infection study. Both studies were carried out in the Leiden University Medical Center (LUMC), Leiden, from 2019 to 2022. The study was approved by the LUMC Institutional Medical Ethical Research Committee (Institutional Review Board P16.111 and P20.015). It was performed according to the European Clinical Trial Directive 2001/20/EC in accordance with International Council for Harmonisation of Technical Requirements for Pharmaceuticals for Human Use Good Clinical Practice (ICH-GCP) guidelines and the Declaration of Helsinki. Written informed consent was obtained from all participants, and possible consequences of the study were explained. Both studies were open-label dose escalation trials, and blinding was not performed. Detailed inclusion and exclusion criteria are found in the previous publications (*3*, *5*). Baseline characteristics of participants in the male cercaria infection study include age in years, median (range): 24 (*18*–*38*); sex, *n* (%): 4 for males (28%) and 10 for females (71%) (*3*). Baseline characteristics of participants in the female cercaria infection study include age in years, median (range): 26 (*18*–*38*); sex, *n* (%): 5 for males (38%) and 8 for females (62%) (*5*).

PBMC cryopreservation and thawing

Heparinized venous blood was diluted 2× in Hanks' balanced salt solution (Thermo Fisher Scientific) containing penicillin G sodium (100 U/ml; Euroco-Pharma BV) and streptomycin (100 μg/ml; Sigma-Aldrich). Density separation was performed, with 10 ml of Ficoll (Apotheek LUMC) added below diluted blood, and samples were centrifuged (400*g* for 25 min, low brake). PBMCs were collected, washed, and cryopreserved in freezing medium: 20% of heat-inactivated fetal bovine serum (FBS; Bodinco) and 10% dimethyl sulfoxide (Millipore) in complete RPMI [RPMI 1640 (Invitrogen) containing pyruvate (1 mM; Sigma-Aldrich), L-glutamine (2 mM; Sigma-Aldrich), penicillin G sodium (100 U/ml; Euroco-Pharma BV), and streptomycin (100 μg/ml; Sigma-Aldrich)]. Cells in freezing medium were placed in a Nalgene Mr. Frosty freezing container (Thermo Fisher Scientific) overnight at −80°C before liquid nitrogen storage. PBMC samples were cryopreserved within 6 hours after blood collection.

Mass cytometry

Before mass cytometry staining, cryopreserved PBMCs were thawed at 37°C in 50% FBS/complete RPMI, washed twice in 10% FBS/complete RPMI, and then placed on ice. Three million cells were transferred to 5-ml microcentrifuge tubes (Eppendorf) for direct nonstimulated staining or 5-ml round-bottom falcon tubes (BD Biosciences) for PMA/ionomycin stimulation. Stimulated cells were incubated for 6 hours at 37°C with PMA (100 ng/ml; Sigma-Aldrich) and ionomycin (1 μg/ml; Sigma-Aldrich), with brefeldin A (10 μg/ml; Sigma-Aldrich) added for the final 4 hours.

Stimulated and nonstimulated cells were then washed twice in Maxpar staining buffer (Fluidigm). All washes during extracellular staining were performed at 400*g* for 5 to 7 min. For the male infection study, a barcode mix targeting β_2-microglobulin and CD298 was added to each individual sample in a six-choose-two scheme using palladiums 104, 106, 108, and 110 and platinums 194 and 198 for 30 min at room temperature (RT). For the female infection study, a barcode mix targeting β_2-microglobulin was added to each individual sample in a six-choose-three scheme using cadmiums 106, 110, 111, 112, 114, and 116 for 30 min at RT. Cells were washed twice in staining buffer and combined into batches of 6 to 20 samples, including one reference per batch. Batched cells were incubated in 1 ml of 500× diluted 500 μM Cell-ID Intercalator-^{103}Rh (Fluidigm) for 15 min at RT. Cells were then washed in staining buffer and resuspended in staining buffer with 5% human TruStain FcX Fc receptor blocking solution (BioLegend) added for 10 min at RT. Metal-conjugated antibodies for extracellular antigens (detailed in tables S1 and S2) were then added for 45 min at RT. Cells were washed twice with staining buffer, and from this point, stimulated and nonstimulated cells were treated differently.

For the nonstimulated panel in the female infection study, cells were fixed in 1.6% formaldehyde (Pierce) for 10 min at RT before permeabilization. In the male study, this step was skipped, and cells went straight to permeabilization with freshly prepared Fix/Perm (eBioscience Foxp3/Transcription Factor Staining Buffer set, following the manufacturer's instructions) for 30 to 45 min at 4°C. Cells were then washed twice in Perm buffer (eBioscience Foxp3/Transcription Factor Staining Buffer set, following the manufacturer's instructions). This and all subsequent washes were performed at 800*g* for 5 to 7 min. Metal-conjugated antibodies for intranuclear antigens (detailed in table S1) were then added in Perm buffer for 30 min at RT.

For the stimulated panel in the female infection study, cells were fixed in 4% formaldehyde (Pierce) for 10 min at RT before permeabilization. In the male infection study, this step was skipped, and the cells went straight to permeabilization with MaxPar Fix I Buffer (Fluidigm, following the manufacturer's instructions) for 20 min at RT. Cells were then washed twice with MaxPar Perm-S Buffer (Fluidigm, following the manufacturer's instructions) before addition of metal-conjugated antibodies (detailed in table S2) for intracellular staining for 30 min at RT. After intracellular staining, cells were washed twice with staining buffer.

After staining, stimulated and nonstimulated cells were fixed with 1.6 to 4% formaldehyde (Pierce) for 10 min at RT. Cells were washed, and 125 μM Cell-ID Intercalator-Ir (Fluidigm) was added in MaxPar Fix and Perm buffer (Fluidigm) overnight at 4°C. The following day cells were washed twice in staining buffer before cryopreservation as performed on fresh samples.

All time points from one participant were stained and measured together in a total of 11 batches, 7 in the male infection study and 4 in the female infection study. Inclusion of a reference PBMC in each batch allowed for quality control, ensuring comparability between batches. Samples were measured with a Helios cytometry by time of flight (CyTOF) mass cytometer (Fluidigm) with wide bore, tuned according to Fluidigm's recommendations. Before acquisition, cells were thawed in RPMI 50% FBS, washed in RPMI, and counted. Cells were resuspended in cell acquisition solution (Fluidigm) in the male study and water in the female study containing 10% EQ Beads (Fluidigm) for acquisition. Next to channels used to detect antibodies, channels for intercalators (^{103}Rh, ^{191}Ir, and ^{193}Ir), calibration beads (^{140}Ce, ^{151}Eu, ^{153}Eu, ^{165}Ho, and ^{175}Lu), and background/contamination (^{131}Xe, ^{133}Cs, ^{138}Ba, ^{206}Pb, and ^{208}Pb) were acquired. FCS files were normalized and concatenated in Helios software, without removing beads.

Mass cytometry data analysis

After normalization, the FCS files were autogated on the Gaussian parameters using cytoflean (v10.3) (*56*). Subsequently, gates were set to select single, live, CD45$^+$ cells for each batch using the openCyto package in R (fig. S11). In the last two steps, the batch FCS files were compensated and debarcoded using the CATALYST package in R (v1.16.2) (*57*). First, the compensation was performed using the nonnegative linear least squares method, provided with a self-measured spillover matrix. Last, the single FCS files per sample were acquired by the default debarcoding pipeline provided by CATALYST.

To account for variation between batches stained and acquired at different times, batch correction was performed using the CytoNorm package (v1.16.2) (*58*). This approach first clusters the data before and performs batch correction within each cluster, with $k = 10$ chosen for the nonstimulated panel and $k = 5$ chosen for the PMA/ionomycin-stimulated panel. For each approach, reference samples used for correction were produced by randomly sampling 200,000 cells from each batch. Quality of the batch correction was assessed, and representative *t*-distributed stochastic neighbor embedding (t-SNE) plots before and after batch correction are shown in fig. S12.

To explore the mass cytometry data, produced samples were clustered and visualized in a two-dimensional t-SNE map. Clustering was performed on the basis of expression of all surface and intracellular antigens using a two-step method. First, cell expression was mapped onto a 15-by-15 SOM grid using the Kohonen package (v3.0.11) (*59*). The SOM grid was then divided into metaclusters using hierarchical clustering, with $k = 70$ clusters chosen for the unstimulated panel and stimulated panel. The number of clusters was chosen by balancing the number of clusters against the silhouette index, where we tried to maximize the amount of immunological relevant clusters until the point where the silhouette index was only linearly decreasing (fig. S13). Clusters were manually assigned to cell lineages on the basis of expression of well-defined lineage markers. Heatmaps of cluster marker expression were produced using the package cytofast (v1.3.3) (*60*). To understand the overall structure of the data, cells (downsampled to 4000 cells per sample) were placed on a t-SNE map using the fast Fourier transform–accelerated interpolation-based t-SNE algorithm (v1.2.1) (*61*). For visualization, this map was then binned using the hexbin package (v3.0.11) (*62*) with 150 bins, allowing assessment of cell lineages, clusters, or marker expression.

For PCA, cell frequencies were scaled to have unit variance. To address the repeated measurement design, we applied the multilevel approach implemented in the Mixomics package (*63*). In this fashion, we tried to minimize the variance between volunteers and focused on variation introduced by clinical outcomes.

Flow cytometry

PBMC samples were used from 12 volunteers at week 16 after infection, equally split between male and female cercaria infections and symptom status. Before flow cytometry staining, cryopreserved PBMCs were thawed at 37°C in 50% FBS/complete RPMI, washed twice in 10% FBS/complete RPMI, and then placed on ice. One million cells per condition were incubated for 24 hours at 37°C with AWA (50 μg/ml) or medium, with brefeldin A (10 μg/ml; Sigma-Aldrich) added for the last 4 hours.

Cells were moved to a v-bottom plate and washed twice in phosphate-buffered saline (PBS) before addition of Live/Dead blue (L23105, Thermo Fisher Scientific) for 20 min at RT. All washes were performed at 400*g* at 4°C for 4 min. Cells were then washed once with 1% bovine serum albumin in PBS. Fluorescent-conjugated antibodies were then added for 1 hour at 4°C (detailed in table S3). Cells were washed twice with 1% bovine serum albumin in PBS before permeabilization with freshly prepared Fix/Perm (eBioscience Foxp3/Transcription Factor Staining Buffer set, following the manufacturer's instructions) for 30 min at 4°C. Cells were then washed twice in Perm buffer (eBioscience Foxp3/Transcription Factor Staining Buffer set, following the manufacturer's instructions). Fluorescent-conjugated antibodies for intracellular antigens (detailed in table S3) were then added in Perm buffer overnight at 4°C. Cells were then washed twice in Perm buffer before acquisition on a five-laser Aurora spectral flow cytometer (Cytek). Gating schemes are shown in fig. S7.

Serum cytokine analyses

Serum cytokine analysis was performed using the Olink platform. Serum samples were run at Olink in Uppsala (Sweden) or University Medical Center Utrecht (Netherlands) using the Olink Target 96 inflammation panel covering 92 different proteins. Data are reported as NPX, an arbitrary unit (AU) on a $\log_2$ scale. Values below the limit of detection (LOD) were extrapolated and included in analysis. Most proteins (66 of 92) had all values above the LOD, with 16 proteins detectable in more than 50% of samples [IL-6, fibroblast growth factor–21 (FGF-21), IL-15RA, monocyte chemotactic protein 3 (MCP-3), neurotrophin-3 (NT-3), FGF-5, sulfotransferase family 1A member 1 (ST1A1), sirtuin 2 (SIRT2), neurturin (NRTN), IL-2RB, thymic stromal lymphopoietin (TSLP), IL-24, glial cell line–derived neurotrophic factor, ARTN, IL-4, and IL-20] and 10 proteins detectable in less than 50% of samples (IL-13, IL-20RA, IL-22RA1, IL-5, LIF, FGF-23, IL-1α, IL-2, IL-33, β subunit of nerve growth factor).

Statistical analyses

A similar modeling strategy was used for the different modalities of data we acquired. For the cellular analysis, we used cluster frequencies as the primary outcome, and for the serum cytokine data, each single target was considered. In this univariate fashion, a generalized linear mixed model was used with sex (of volunteer), time point (in weeks, as factor), and symptoms (dichotomous) as explanatory variables. As random effects, both volunteer and study were added as random intercept. To match the nature of the data, a Gaussian family was considered for the serum cytokine data and a binomial

family with logit link for the cellular data. The frequency and weights for the binomial model were based on the $CD45^+$ cells for the unstimulated data and for the PMA-stimulated data $CD45^+$ and cytokine-positive cells. To deal with any under- and overdispersion, an extra random intercept for sample ID was added to the models for the cellular data. From the generated models, the estimates together with their *P* values (*t*-statistic, via Satterthwaite's degrees of freedom method) were extracted. Afterward, for each modality of data, all *P* values from the generated models were corrected with the Benjamini-Hochberg procedure. Adjusted *P* values with an FDR of <0.05 were considered significant. Analysis was performed in R (v4.2.1) (*64*) with the lme4 (v1.1) (*65*) and lmerTest (v3.1) (*66*) packages.

The correlation analysis between the stimulated cellular data and the serum data was performed on only a significant (FDR < 0.05) subset of clusters and proteins. For each week containing data from both studies (weeks 0, 4, and 8), a correlation matrix was constructed on the basis of Spearman's correlation. A significant association deviating from zero was tested for each pair of cluster and protein. For each week, the resulting *P* values were corrected with the Benjamini-Hochberg procedure. All data points represent one biological replicate (total: $n = 27$ for cellular data and $n = 30$ for serum cytokine data), and technical replicates were not performed. No sample points were omitted from analysis. All testing was two sided.

Supplementary Materials

The PDF file includes:
Figs. S1 to S13
Tables S1 to S3

Other Supplementary Material for this manuscript includes the following:
Data file S1
MDAR Reproducibility Checklist

REFERENCES AND NOTES

1. D. G. Colley, A. L. Bustinduy, W. E. Secor, C. H. King, Human schistosomiasis. *Lancet* **383**, 2253–2264 (2014).
2. A. G. Ross, D. Vickers, G. R. Olds, S. M. Shah, D. P. McManus, Katayama syndrome. *Lancet Infect. Dis.* **7**, 218–224 (2007).
3. M. C. C. Langenberg, M.-A. Hoogerwerf, J. P. R. Koopman, J. J. Janse, J. Kos-van Oosterhoud, C. Feijt, S. P. Jochems, C. J. de Dood, R. van Schuijlenburg, A. Ozir-Fazalalikhan, M. D. Manurung, E. Sartono, M. T. van der Beek, B. M. F. Winkel, P. H. Verbeek-Menken, K. A. Stam, F. W. B. van Leeuwen, P. Meij, A. van Diepen, L. van Lieshout, G. J. van Dam, P. L. A. M. Corstjens, C. H. Hokke, M. Yazdanbakhsh, L. G. Visser, M. Roestenberg, A controlled human *Schistosoma mansoni* infection model to advance novel drugs, vaccines and diagnostics. *Nat. Med.* **26**, 326–332 (2020).
4. M. C. C. Langenberg, M.-A. Hoogerwerf, J. J. Janse, L. van Lieshout, P. L. A. M. Corstjens, M. Roestenberg, CoHSI clinical trial team, Katayama syndrome without *Schistosoma mansoni* eggs. *Ann. Intern. Med.* **170**, 732 (2019).
5. J. P. R. Koopman, E. L. Houlder, J. J. Janse, M. Casacuberta-Partal, O. A. C. Lamers, J. C. Sijtsma, C. de Dood, S. T. Hilt, A. Ozir-Fazalalikhan, V. P. Kuiper, G. V. T. Roozen, L. M. de Bes-Roeleveld, Y. C. M. Kruize, L. J. Wammes, H. H. Smits, L. van Lieshout, G. J. van Dam, I. M. van Amerongen-Westra, P. Meij, P. L. A. M. Corstjens, S. P. Jochems, A. van Diepen, M. Yazdanbakhsh, C. H. Hokke, M. Roestenberg, Safety and infectivity of female cercariae in *Schistosoma*-naïve, healthy participants: A controlled human *Schistosoma mansoni* infection study. *EBioMedicine* **97**, 104832 (2023).
6. M. A. Verjee, Schistosomiasis: Still a cause of significant morbidity and mortality. *Res. Rep. Trop. Med.* **10**, 153–163 (2019).
7. A. Nalugwa, F. Nuwaha, E. M. Tukahebwa, A. Olsen, Single versus double dose praziquantel comparison on efficacy and *Schistosoma mansoni* re-infection in preschool-age children in Uganda: A randomized controlled trial. *PLOS Negl. Trop. Dis.* **9**, e0003796 (2015).
8. A. P. Mountford, R. Harrop, Vaccination against schistosomiasis: The case for lung-stage antigens. *Parasitol. Today* **14**, 109–114 (1998).
9. A. R. de Jesus, A. Silva, L. B. Santaa, A. Magalhães, A. A. de Jesus, R. P. de Almeida, M. A. V. Rêgo, M. N. Burattini, E. J. Pearce, E. M. Carvalho, Clinical and immunologic evaluation of 31 patients with acute schistosomiasis mansoni. *J. Infect. Dis.* **185**, 98–105 (2002).
10. J. M. Grzych, E. Pearce, A. Cheever, Z. A. Caulada, P. Caspar, S. Heiny, F. Lewis, A. Sher, Egg deposition is the major stimulus for the production of Th2 cytokines in murine schistosomiasis mansoni. *J. Immunol.* **146**, 1322–1327 (1991).
11. L. A. de Oliveira Fraga, M. N. Torrero, A. S. Tocheva, E. Mitre, S. J. Davies, Induction of type 2 responses by schistosome worms during prepatent infection. *J. Infect. Dis.* **201**, 464–472 (2010).
12. A. H. Costain, A. T. Phythian-Adams, S. A. P. Colombo, A. K. Marley, C. Owusu, P. C. Cook, S. L. Brown, L. M. Webb, R. J. Lundie, H. H. Smits, M. Berriman, A. S. MacDonald, Dynamics of host immune response development during *Schistosoma mansoni* infection. *Front. Immunol.* **13**, 906338 (2022).
13. E. L. Houlder, A. H. Costain, I. Nambuya, S. L. Brown, J. P. R. Koopman, M. C. C. Langenberg, J. J. Janse, M. A. Hoogerwerf, A. J. L. Ridley, J. E. Forde-Thomas, S. A. P. Colombo, B. M. F. Winkel, A. A. Galdon, K. F. Hoffmann, P. C. Cook, M. Roestenberg, H. Mpairwe, A. S. MacDonald, Pulmonary inflammation promoted by type-2 dendritic cells is a feature of human and murine schistosomiasis. *Nat. Commun.* **14**, 1863 (2023).
14. M. Sombetzki, C. Reinholdt, F. Winkelmann, A. Rabes, N. Koslowski, E. C. Reisinger, A one-year unisexual *Schistosoma mansoni* infection causes pathologic organ alterations and persistent non-polarized T cell-mediated inflammation in mice. *Front. Immunol.* **13**, 1010932 (2022).
15. N. Koslowski, M. Sombetzki, M. Loebermann, R. Engelmann, N. Grabow, C. H. Osterreicher, M. Trauner, B. Mueller-Hilke, E. C. Reisinger, Single-sex infection with female *Schistosoma mansoni* cercariae mitigates hepatic fibrosis after secondary infection. *PLOS Negl. Trop. Dis.* **11**, e0005595 (2017).
16. J. Boissier, K. Chlichlia, Y. Digon, A. Ruppel, H. Moné, Preliminary study on sex-related inflammatory reactions in mice infected with *Schistosoma mansoni*. *Parasitol. Res.* **91**, 144–150 (2003).
17. M. A. L. Picard, J. Boissier, D. Roquis, C. Grunau, J. F. Allienne, D. Duval, E. Toulza, N. Arancibia, C. R. Caffrey, T. Long, S. Nidelet, M. Rohmer, C. Cosseau, Sex-biased transcriptome of *Schistosoma mansoni*: Host-parasite interaction, genetic determinants and epigenetic regulators are associated with sexual differentiation. *PLOS Negl. Trop. Dis.* **10**, e0004930 (2016).
18. J. M. Fitzpatrick, K. F. Hoffmann, Dioecious *Schistosoma mansoni* express divergent gene repertoires regulated by pairing. *Int. J. Parasitol.* **36**, 1081–1089 (2006).
19. L. L. Lanier, A. M. Le, C. I. Civin, M. R. Loken, J. H. Phillips, The relationship of Cd16 (Leu-11) and Leu-19 (NKH-1) antigen expression on human peripheral blood NK cells and cytotoxic T lymphocytes. *J. Immunol.* **136**, 4480–4486 (1986).
20. J. R. Groom, A. D. Luster, CXCR3 in T cell function. *Exp. Cell Res.* **317**, 620–631 (2011).
21. T. Haug, M. Aigner, M. M. Peuser, C. D. Strobl, K. Hildner, D. Mougiakakos, H. Bruns, A. Mackensen, S. Völkl, Human double-negative regulatory T-cells induce a metabolic and functional switch in effector T-cells by suppressing mTOR activity. *Front. Immunol.* **10**, 883 (2019).
22. K. J. Young, B. DuTemple, M. J. Phillips, L. Zhang, Inhibition of graft-versus-host disease by double-negative regulatory T cells. *J. Immunol.* **171**, 134–141 (2003).
23. R. Collin, V. Dugas, A. N. Pelletier, G. Chabot-Roy, S. Lesage, The mouse Idd2 locus is linked to the proportion of immunoregulatory double-negative T cells, a trait associated with autoimmune diabetes resistance. *J. Immunol.* **193**, 3503–3512 (2014).
24. J. L. Karnell, V. Kumar, J. Y. Wang, S. Wang, E. Voynova, R. Ettinger, Role of $CD11c^+$ $T\text{-}bet^+$ B cells in human health and disease. *Cell. Immunol.* **321**, 40–45 (2017).
25. K. de Ruiter, S. P. Jochems, D. L. Tahapary, K. A. Stam, M. König, V. van Unen, S. Laban, T. Höllt, M. Mbow, B. P. F. Lelieveldt, F. Koning, E. Sartono, J. W. A. Smit, T. Supali, M. Yazdanbakhsh, Helminth infections drive heterogeneity in human type 2 and regulatory cells. *Sci. Transl. Med.* **12**, eaaw3703 (2020).
26. T. Michel, A. Poli, A. Cuapio, B. Briquemont, G. Iserentant, M. Ollert, J. Zimmer, Human $CD56^{bright}$ NK cells: An update. *J. Immunol.* **196**, 2923–2931 (2016).
27. N. W. Zwirner, C. I. Domaica, M. B. Fuertes, Regulatory functions of NK cells during infections and cancer. *J. Leukoc. Biol.* **109**, 185–194 (2021).
28. M. Pascual-Garcia, E. Bonfill-Teixidor, E. Planas-Rigol, C. Rubio-Perez, R. Ludaro, A. Arias, I. Cuartas, A. Sala-Hojman, L. Escudero, F. Martínez-Ricarte, I. Huber-Ruano, P. Nuciforo, L. Pedrosa, C. Marques, I. Braña, E. Garralda, M. Vieito, M. Squatrito, E. Pineda, F. Graus, C. EspejoH, J. Sahuquillo, J. Tabernero, J. Seoane, LIF regulates CXCL9 in tumor-associated macrophages and prevents $CD8^+$ T cell tumor-infiltration impairing anti-PD1 therapy. *Nat. Commun.* **10**, 2416 (2019).
29. A. Itoh, L. Ortiz, K. Kachapati, Y. H. Wu, D. Adams, K. Bednar, S. Mukherjee, C. Chougnet, R. S. Mittler, Y.-G. Chen, L. Dolan, W. M. Ridgway, Soluble CD137 ameliorates acute type 1 diabetes by inducing T cell anergy. *Front. Immunol.* **10**, 2566 (2019).
30. K. Kamat, V. Krishnan, O. Dorigo, Macrophage-derived CCL23 upregulates expression of T-cell exhaustion markers in ovarian cancer. *Br. J. Cancer* **127**, 1026–1033 (2022).
31. A. Wangwiwatsin, A. V. Protasio, S. Wilson, C. Owusu, N. E. Holroyd, M. J. Sanders, J. Keane, M. J. Doenhoff, G. Rinaldi, M. Berriman, Transcriptome of the parasitic flatworm

Schistosoma mansoni during intra-mammalian development. *PLOS Negl. Trop. Dis.* **14**, e0007743 (2020).
32. P. F. Basch, Cultivation of *Schistosoma mansoni* in vitro. I. Establishment of cultures from cercariae and development until pairing. *J. Parasitol.* **67**, 179–185 (1981).
33. S. A. Amici, N. A. Young, J. Narvaez-Miranda, K. A. Jablonski, J. Arcos, L. Rosas, T. L. Papenfuss, J. B. Torrelles, W. N. Jarjour, M. Guerau-de-Arellano, CD38 is robustly induced in human macrophages and monocytes in inflammatory conditions. *Front. Immunol.* **9**, 1593 (2018).
34. C. Dentone, D. Fenoglio, A. Parodi, T. Altosole, A. Di Biagio, F. Bozzano, G. Nasi, A. Vena, M. Fabbi, F. Ferrera, B. Bruzzone, M. Giacomini, D. R. Giacobbe, P. Pelosi, A. De Maria, M. Bassetti, R. De Palma, G. Filaci, Intermediate monocytes expansion and homing markers expression in COVID-19 patients associate with kidney dysfunction. *Clin. Exp. Med.* **23**, 1235–1242 (2023).
35. F. R. Toapanta, P. J. Bernal, S. Fresnay, T. C. Darton, C. Jones, C. S. Waddington, C. J. Blohmke, G. Dougan, B. Angus, M. M. Levine, A. J. Pollard, M. B. Sztein, Oral wild-type salmonella typhi challenge induces activation of circulating monocytes and dendritic cells in individuals who develop typhoid disease. *PLOS Negl. Trop. Dis.* **9**, e0003837 (2015).
36. R. Tippalagama, A. Singhania, P. Dubelko, C. S. Lindestam Arlehamn, A. Crinklaw, M. Pomaznoy, G. Seumois, A. D. deSilva, S. Premawansa, D. Vidanagama, B. Gunasena, N. D. S. Goonawardhana, D. Ariyaratne, T. J. Scriba, R. H. Gilman, M. Saito, R. Taplitz, P. Vijayanand, A. Sette, B. Peters, J. G. Burel, HLA-DR marks recently divided antigen-specific effector CD4 T cells in active tuberculosis patients. *J. Immunol.* **207**, 523–533 (2021).
37. J. Reed, M. Reichelt, S. A. Wetzel, Lymphocytes and trogocytosis-mediated signaling. *Cells* **10**, 1478 (2021).
38. J. Reed, S. A. Wetzel, Trogocytosis-mediated intracellular signaling in $CD4^+$ T cells drives T_H2-associated effector cytokine production and differentiation. *J. Immunol.* **202**, 2873–2887 (2019).
39. M. L. Liu, S. C. Guo, J. M. Hibbert, V. Jain, N. Singh, N. O. Wilson, J. K. Stiles, CXCL10/IP-10 in infectious diseases pathogenesis and potential therapeutic implications. *Cytokine Growth Factor Rev.* **22**, 121–130 (2011).
40. M. G. Netea, B. J. Kullberg, J. W. M. Van der Meer, Circulating cytokines as mediators of fever. *Clin. Infect. Dis.* **31**, S178–S184 (2000).
41. A. D. Luster, J. C. Unkeless, J. V. Ravetch, Gamma-interferon transcriptionally regulates an early-response gene containing homology to platelet proteins. *Nature* **315**, 672–676 (1985).
42. E. J. Pearce, A. S. Macdonald, The immunobiology of schistosomiasis. *Nat. Rev. Immunol.* **2**, 499–511 (2002).
43. S. A. Redpath, N. van der Werf, A. S. MacDonald, R. M. Maizels, M. D. Taylor, *Schistosoma mansoni* larvae do not expand or activate $Foxp3^+$ regulatory T cells during their migratory phase. *Infect. Immun.* **83**, 3881–3889 (2015).
44. D. B. R. Herbert, T. Orekov, C. Perkins, F. D. Finkelman, IL-10 and TGF-β redundantly protect against severe liver injury and mortality during acute schistosomiasis. *J. Immunol.* **181**, 7214–7220 (2008).
45. M. Hesse, C. A. Piccirillo, Y. Belkaid, J. Prufer, M. Mentink-Kane, M. Leusink, A. W. Cheever, E. M. Shevach, T. A. Wynn, the pathogenesis of schistosomiasis is controlled by cooperating IL-10-producing innate effector and regulatory T cells. *J. Immunol.* **172**, 3157–3166 (2004).
46. C. T. Prendergast, D. E. Sanin, P. C. Cook, A. P. Mountford, $CD4^+$ T cell hyporesponsiveness after repeated exposure to *Schistosoma mansoni* larvae is dependent upon interleukin-10. *Infect. Immun.* **83**, 1418–1430 (2015).
47. L. E. P. M. van der Vlugt, K. Obieglo, A. Ozir-Fazalalikhan, T. Sparwasser, S. Haeberlein, H. H. Smits, Schistosome-induced pulmonary B cells inhibit allergic airway inflammation and display a reduced Th2-driving function. *Int. J. Parasitol.* **47**, 545–554 (2017).
48. A. Vecchie, A. Bonaventura, S. Toldo, L. Dagna, C. A. Dinarello, A. Abbate, IL-18 and infections: Is there a role for targeted therapies? *J. Cell. Physiol.* **236**, 1638–1657 (2021).
49. F. Toulza, L. Tsang, T. H. M. Ottenhoff, M. Brown, H. M. Dockrell, *Mycobacterium tuberculosis*-specific $CD4^+$ T-cell response is increased, and Treg cells decreased, in anthelmintic-treated patients with latent TB. *Eur. J. Immunol.* **46**, 752–761 (2016).
50. Y. Schmiedel, G. Mombo-Ngoma, L. A. Labuda, J. J. Janse, B. de Gier, A. A. Adegnika, S. Issifou, P. G. Kremsner, H. H. Smits, M. Yazdanbakhsh, $CD4^+$ $CD25^{hi}FOXP3^+$ regulatory T cells and cytokine responses in human schistosomiasis before and after treatment with praziquantel. *PLOS Negl. Trop. Dis.* **9**, e0003995 (2015).
51. E. van Riet, F. C. Hartgers, M. Yazdanbakhsh, Chronic helminth infections induce immunomodulation: Consequences and mechanisms. *Immunobiology* **212**, 475–490 (2007).
52. R. M. Maizels, H. J. McSorley, Regulation of the host immune system by helminth parasites. *J. Allergy Clin. Immunol.* **138**, 666–675 (2016).
53. S. Logan, M. Armstrong, E. Moore, G. Nebbia, J. Jarvis, M. Suvari, J. Bligh, P. L. Chiodini, M. Brown, T. Doherty, Acute schistosomiasis in travelers: 14 years' experience at the hospital for tropical diseases, London. *Am. J. Trop. Med. Hyg.* **88**, 1032–1034 (2013).
54. E. Driciru, J. P. R. Koopman, S. Cose, A. A. Siddiqui, M. Yazdanbakhsh, A. M. Elliott, M. Roestenberg, Immunological considerations for schistosoma vaccine development: Transitioning to endemic settings. *Front. Immunol.* **12**, 635985 (2021).
55. S. Jauréguiberry, L. Paris, E. Caumes, Acute schistosomiasis, a diagnostic and therapeutic challenge. *Clin. Microbiol. Infect.* **16**, 225–231 (2010).
56. JimboMahoney/cytofclean: Automatically cleans mass cytometry (CyTOF) FCS files. R package version 1.0.3 (2021); https://github.com/JimboMahoney/cytofclean.
57. H. L. Crowell, V. R. T. Zanotelli, S. Chevrier, M. D. Robinson, CATALYST: Cytometry dATa anALYSis Tools. R package version 1.16.2 (2021); https://github.com/HelenaLC/CATALYST.
58. S. Van Gassen, B. Gaudilliere, M. S. Angst, Y. Saeys, N. Aghaeepour, CytoNorm: A normalization algorithm for cytometry data. *Cytometry A* **97**, 268–278 (2020).
59. R. Wehrens, J. Kruisselbrink, Flexible self-organizing maps in kohonen 3.0. *J. Stat. Softw.* **87**, 1–18 (2018).
60. G. Beyrend, K. Stam, T. Hollt, F. Ossendorp, R. Arens, Cytofast: A workflow for visual and quantitative analysis of flow and mass cytometry data to discover immune signatures and correlations. *Comput. Struct. Biotec.* **16**, 435–442 (2018).
61. G. C. Linderman, M. Rachh, J. G. Hoskins, S. Steinerberger, Y. Kluger, Fast interpolation-based t-SNE for improved visualization of single-cell RNA-seq data. *Nat. Methods* **16**, 243–245 (2019).
62. D. Carr, D. Lewin-Koh, M. Maechler, D. Sarkar, hexbin: Hexagonal binning routines. R package version 1.28.3 (2021).
63. F. Rohart, B. Gautier, A. Singh, K. A. Le Cao, mixOmics: An R package for 'omics feature selection and multiple data integration. *PLOS Comput. Biol.* **13**, e1005752 (2017).
64. R Core Team. R: A language and environment for statistical computing (R Foundation for Statistical Computing, Vienna, Austria, 2021).
65. D. Bates, M. Machler, B. M. Bolker, S. C. Walker, Fitting linear mixed-effects models using lme4. *J. Stat. Softw.* **67**, 1–48 (2015).
66. A. Kuznetsova, P. B. Brockhoff, R. H. B. Christensen, lmerTest package: Tests in linear mixed effects models. *J. Stat. Softw.* **82**, 1–26 (2017).

Acknowledgments: We thank P. van Genderen, A. Bustinduy, and A. Wajja for valuable advice as members of the safety monitoring committee. We thank O. A. C. Lamers, C. de Dood, S. T. Hilt, A. Ozir-Fazalalikhan, V. P. Kuiper, G. V. T. Roozen, L. Wammes, L. van Lieshout, G. J. van Dam, I. M. Amerongen-Westra, P. Meij, P. L. A. M. Corstjens, S. P. Jochems, A. van Diepen, C. H. Hokke, M. A. A. Erkens, J. L. Fehrmann-Naumann, M. S. Ganesh, H. Gerritsma, G. C. Hardeman, P. T. Hoekstra-Mevius, Y. D. Mouwenda, H. H. Smits, K. Suijk-Benschop, J. J. C. de Vries, and C. J. G. van Zeijl-van der Ham for laboratory, clinical, and data-analyzing support during the study. Most of all, we thank all volunteers participating in the study, without whom the study could not have been performed. **Funding:** This project has received funding from the European Union's Horizon 2020 research and innovation programme under grant agreement no. 815643. M.Y. was supported by a NWO Spinoza prize 2021, a NWO-WOTRO Science for Global Development Programme (no. W 07.30318.019), and an ERC advanced grant. M.R. was supported by a NWO Veni grant (no. 016.156.076) and a Development and a Gisela Thier Fellowship (no. 14-0645) from LUMC. E.L.H. was supported by a HIC-Vac pump priming award, Merck Schistosomiasis Research Grant, and the European Union's Horizon 2020 research and innovation programme under the Marie Skłodowska-Curie grant (101063914). This study is part of the EDCTP2 programme supported by the European Union. **Author contributions:** M.Y., M.R., K.A.S., and E.L.H. were responsible for the study design. K.A.S. and E.L.H. were responsible for the statistical analysis and data interpretation and prepared the first draft. M.Y., M.R., and E.L.H. acquired funding. M.-A.H., J.P.R.K., M.C.C.L., and M.R. were the clinical investigators. J.J.J. performed the trial management. M.C.P., J.C.S., and J.J.J. were responsible for the production and release of cercariae. M.H.K., E.L.H., P.N., and F.S. generated the data and optimized the experimental protocols. L.H.M.d.B.-R. and Y.C.M.K. coordinated PBMC sample collection. All authors reviewed the manuscript. **Competing interests:** The authors declare that they have no competing interests. The funding sources had no role in collecting, analyzing, interpreting, or reporting the data. The opinions expressed in this document reflect only the author's view. The funding sources are not responsible for any use that may be made of the information that it contains. **Data and materials availability:** All data needed to support the conclusions of the paper are present in the paper or the Supplementary Materials (data file S1). All materials used in the paper are commercially available without a material transfer agreement.

Submitted 13 October 2023
Accepted 7 June 2024
Published 5 July 2024
10.1126/sciimmunol.adl1965